

An LLM Driven Agent Framework for Automated Infrared Spectral Multi Task Reasoning

Zujie Xie^{a,†}, Zixuan Chen^{a,†}, Jiheng Liang^a, Xiangyang Yu^a, Ziru Yu^{b,*}

^a School of Physics, State Key Laboratory of Optoelectronic Materials and Technologies, Sun Yat-Sen University, Guangzhou, 510275, China

^b School of electronics and communication engineering, Sun Yat-Sen University, Shenzhen, 518107, China

[†] Zujie Xie and Zixuan Chen contribute equally to the article.

* Correspondence should be addressed to Ziru Yu; Email: yuziru@mail.sysu.edu.cn

Abstract: Infrared spectroscopy offers rapid, non destructive measurement of chemical and material properties but suffers from high dimensional, overlapping spectral bands that challenge conventional chemometric approaches. Emerging large language models (LLMs), with their capacity for generalization and reasoning, offer promising potential for automating complex scientific workflows. Despite this promise, their application in IR spectral analysis remains largely unexplored. This study addresses the critical challenge of achieving accurate, automated infrared spectral interpretation under low-data conditions using an LLM-driven framework. We introduce an end-to-end, large language model driven agent framework that integrates a structured literature knowledge base, automated spectral preprocessing, feature extraction, and multi task reasoning in a unified pipeline. By querying a curated corpus of peer reviewed IR publications, the agent selects scientifically validated routines. The selected methods transform each spectrum into low dimensional feature sets, which are fed into few shot prompt templates for classification, regression, and anomaly detection. A closed loop, multi turn protocol iteratively appends mispredicted samples to the prompt, enabling dynamic refinement of predictions. Across diverse materials: stamp pad ink, Chinese medicine, Pu'er tea, Citri Reticulatae Pericarpium and waste water COD datasets, the multi turn LLM consistently outperforms single turn inference, rivaling or exceeding machine learning and deep learning models under low data regimes. This study introduces a novel integration of LLMs with IR spectroscopy, leveraging structured literature guidance and few-shot learning for automated, high-accuracy spectral interpretation. The framework requires minimal labeled data and dynamically improves performance through iterative prompting, making it particularly valuable in resource-limited settings. By combining domain-specific reasoning with generalizable inference capabilities, this approach establishes a new paradigm for intelligent, scalable infrared spectral analysis across diverse scientific and industrial applications.

Keywords: Spectral analysis; Infrared spectroscopy; Large language models; Few shot learning; Automated chemometrics

1. Introduction

Infrared spectroscopy has emerged as a versatile analytical modality across food quality assessment, pharmaceutical process monitoring, agricultural product evaluation, and environmental sensing. Its non destructive nature, rapid data acquisition, and minimal sample preparation have rendered IR spectroscopy particular attraction for real time, in situ analysis in both academic research and industrial practice[1]. Nonetheless, the intrinsically high dimensionality of IR spectra, coupled with complex and overlapping absorption bands, imposes formidable challenges for robust, generalizable interpretation. Traditional machine learning and deep learning approaches ranging from partial least squares regression and support vector machines to convolutional neural networks and Transformer based architectures have achieved high accuracy on curated datasets through extensive feature engineering, model calibration, and hyperparameter optimization[2]. However, these methods often require large, representative training sets to mitigate overfitting, and they frequently necessitate retraining or recalibration when confronted with novel sample matrices or different instrumentation. Such dependencies introduce substantial costs in data collection and annotation and impede rapid deployment in variable real world environments.

Recent advances in large language models (LLMs) have demonstrated powerful capabilities in few shot learning, chain of

thought reasoning, and cross domain generalization[3][4]. Some pioneering studies have begun to apply LLMs to the scientific field, and LLMs have gradually developed into LLM based scientific agents that can automatically perform key scientific research tasks from hypothesis generation, experimental design to data analysis and simulation[5][6]. Unlike general purpose LLMs, these specialized agents integrate domain knowledge, advanced tool sets, and powerful verification mechanisms, enabling them to handle complex data types, ensure reproducible results, and promote scientific breakthroughs. LLMs are becoming a general tool for connecting computational methods, experimental data, literature text resources, and domain expertise[7]. In the field of spectral analysis and spectral detection, LLMs are often used for narrow tasks of specific substances and rely on customized rapid engineering to convert numerical inputs into interpretable outputs. For example, in the field of aflatoxin B₁ detection, Zhu et al. (2024) used a Babbage 002 large language model finetuned on a subpixel decomposed NIR spectral sequence in JSON format to predict the toxin content, and the results showed that it had higher accuracy than one dimensional and two dimensional CNN methods[8]. In the field of UV-NIR spectroscopy wastewater analysis, Liang et al. (2024) used a large language model to extract characteristic spectral bands for chemical oxygen demand prediction, demonstrating that prompt driven LLM reasoning can match or surpass traditional machine learning methods while greatly reducing the need for task specific parameter tuning[9].

To date, there remains a clear gap in evaluating whether LLMs can be harnessed to automate end-to-end spectral analysis workflows spanning preprocessing, feature extraction, and downstream inference across diverse IR datasets and multiple analytical objectives.

To address these limitations, we propose a unified, LLM driven agent framework that seamlessly integrates literature based method retrieval, automated spectral preprocessing, feature extraction, and multi task reasoning within a single end-to-end pipeline. A structured knowledge base of peer reviewed IR spectroscopy publications is first queried via retrieval algorithms to identify relevant preprocessing and feature extraction methods for the specified research object. These method descriptions are then mapped to a predefined Python function library comprising Asymmetric Least Squares baseline correction, Savitzky-Golay smoothing, standard normal variate transformation, multiplicative scatter correction, normalization, detrending, PCA, NMF, continuous wavelet transform, spectral derivatives, peak detection, and statistical summarization without exposing raw high dimensional spectral arrays to the LLM. The agent invokes the selected functions in sequence to transform the spectral data into structured feature sets, ensuring that each step remains scientifically grounded and reproducible. Figure 1 shows the basic structure of An LLM Driven Agent Framework for Automated Infrared Spectral Multi Task Reasoning.

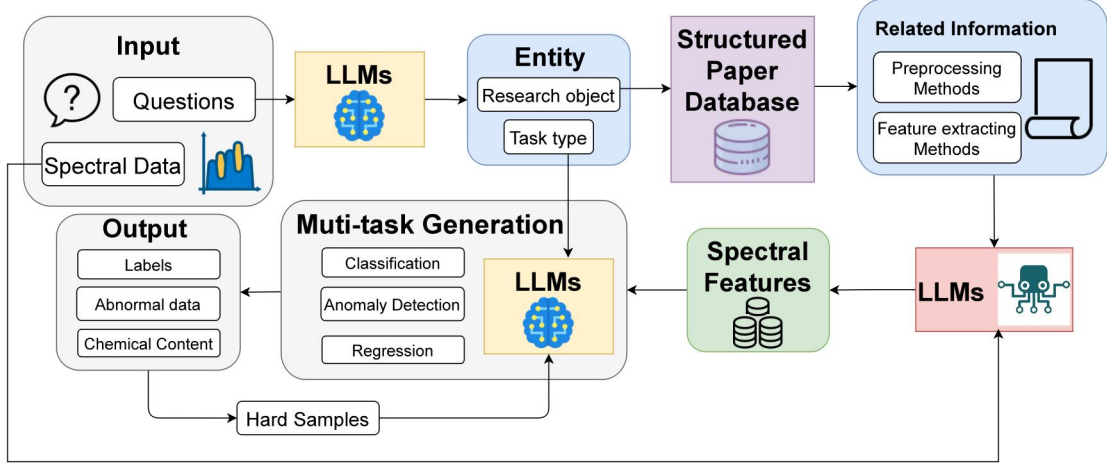


Figure 1. Basic structure of An LLM Driven Agent Framework for Automated infrared Spectral Multi Task Reasoning

Building upon this automated preprocessing and feature extraction backbone, our framework incorporates multi task reasoning capabilities, enabling the LLM to perform downstream analytical tasks such as classification, regression, and anomaly detection within the same conversational context. For each task, the model receives few shot examples drawn from the generated feature sets and iteratively refines its predictions through a closed loop protocol: hard examples identified via misclassification or largest

regression error are appended to the prompt, and performance is continuously monitored using appropriate metrics with early stopping governed by a held out test set. By embedding this multi turn, chain of thought reasoning directly into the agent's workflow, the proposed framework not only automates the selection and execution of chemometric methods but also adapts dynamically to diverse analytical objectives, thus offering a flexible, interpretable, and scalable solution for IR spectral analysis.

The code and parts of data will be made available at <https://github.com/Jeff11272/LLM-Agent-for-Automated-Infrared-Spectral-Reasoning>.

The key contributions of this work are:

1. End-to-end intelligent spectral analysis pipeline. We integrate a priori literature knowledge to select scientifically validated preprocessing and feature-extraction routines, then apply multi-turn LLM inference to execute diverse analytical tasks within a single workflow.
2. Unified multi-task framework. Our system concurrently performs classification, regression, and anomaly detection, overcoming the constraints of single-objective methods.
3. Few-shot prompting efficiency. By leveraging only minimal training data, the agent achieves high accuracy that consistently surpasses traditional machine learning models trained on equivalent sample sizes.
4. Multi-turn conversational enhancement. We demonstrate that iterative prompt refinement significantly strengthens the model's reasoning capabilities across all analytical tasks.

2. Materials and Method

2.1 Experimental materials

This study encompassed three types of spectroscopic tasks: classification, anomaly detection, and regression, each associated with specific sample sets and corresponding wavelength ranges.

For the classification and anomaly detection tasks, four categories of materials were analyzed. In the classification task, the objective was to distinguish between different subclasses within a broad material category, assigning each sample to a specific subclass label. The anomaly detection task, framed as a binary classification problem, aimed to determine whether a given sample belonged to a predefined subclass (True) or not (False).

The first dataset consisted of nine different commercial brands of red stamp pad ink, each formulated with varying chemical compositions. Spectral data were acquired over the 400-1700 nm wavelength range. The second dataset involved three types of Chinese medicinal materials, including *Lonicerae Japonicae Flos* (LJF), *Lonicerae Flos* (LF) and the mixture of them. These samples were analyzed within the 900-1700 nm spectral range. The third dataset comprised fourteen types of *Pu'er* tea collected from different geographical origins across Yunnan Province, China, all harvested in 2022 to ensure consistent climatic and soil conditions. Their spectra were also recorded in the 900-1700 nm range. The fourth dataset included *Citri Reticulatae Pericarpium* (CRP) samples with storage durations ranging from 1 to 8 years, with spectral measurements taken within the 900-1700 nm range.

For the regression task, the goal was to predict the chemical oxygen demand (COD) concentration of water samples. Spectral and COD data were obtained from wastewater collected in Chongqing, China. This dataset included three types of samples: (i) Influent samples taken before treatment at a municipal wastewater treatment plant, (ii) Effluent samples collected post treatment and prior to discharge, and (iii) River water samples collected from nearby natural water bodies. Sample collection was conducted between March 1 and May 15, 2023. Each sample was split into two portions: one for recording the raw absorption spectra and the other for COD concentration determination via the potassium dichromate titration method. The spectral measurements for this dataset covered the 190-1100 nm wavelength range.

Table 1 Experimental material data summary

Sample Name	Class	Difference of classes	Wavelength Range	Task Type
Stamp pad Ink	9	Difference products from different bands	400-1700nm	Classification, Anormal Detection
Chinese Medicine	3	<i>Lonicerae Japonicae Flos</i> (LJF), <i>Lonicerae Flos</i> (LF) and the mixture of them	900-1700nm	Classification, Anormal Detection

Citri Reticulatae Pericarpium	8	Samples with storage durations ranging from 1 to 8 years	900-1700nm	Classification, Anormal Detection
Pu'er Tea	14	Samples with different geographical origins	900-1700nm	Classification, Anormal Detection
Waste Water	3	Influent samples, Effluent samples and River water	190-1100nm	Regression

2.2 Structured Knowledge Base and Entity Retrieval

In order to endow our automated spectral analysis framework with domain specific knowledge, we built upon the Spectral Data Analysis and Application Platform (SDAAP) dataset developed in our prior work, which represents the first systematically curated, open access text corpus dedicated to spectroscopic analysis and detection[10]. SDAAP not only aggregates and annotates peer reviewed publications across diverse spectroscopic applications, but also supplies each record with structured "knowledge guidance" entries that specify experimental targets, spectral modalities, preprocessing protocols, feature extraction techniques, and modeling approaches. This resource addresses a critical deficiency in publicly available text datasets for spectroscopy and provides a solid foundation for subsequent LLM applications in this domain.

From SDAAP, we filtered those entries directly pertinent to the materials examined in the present study namely, commercial stamp pad inks, traditional Chinese medicinal herbs, Pu'er teas, and Citri Reticulatae Pericarpium with the goal of aligning our knowledge base with the experimental materials described in Section 2.1. Each selected paper was parsed using minerU, an automated literature mining tool[11], and the resulting annotations were ingested into an LLM pipeline to extract structured metadata. The extracted fields included the study's material or analyte focus, the specific spectroscopic technique and wavelength bands employed, the best preprocessing workflow applied to the raw spectra, the best feature derivation strategy, and the predictive model architecture used.

Within our end-to-end spectral analysis system, user input comprises two modalities: a natural language query and raw spectral measurements. Upon receiving a query, the system invokes an LLM with a bespoke prompt engineered for entity recognition. The LLM parses the question to identify two key entities: the research object and the analysis task type (classification, anomaly detection, or regression). Once the research object entity is identified, retrieval algorithms are used to search the structured knowledge base for records whose material descriptors match or closely resemble the query entity. The retrieved structured entries are then forwarded, alongside the raw spectral data, to a downstream LLM agent module that synthesizes prior knowledge with the new measurements. Concurrently, the extracted task type entity informs a multi task inference controller within the LLM agent, directing it to apply the appropriate reasoning paradigm whether discriminative classification, binary anomaly detection, or continuous value regression to produce the final analytical output. Figure 2 shows the specific process of entity extraction and knowledge retrieval.

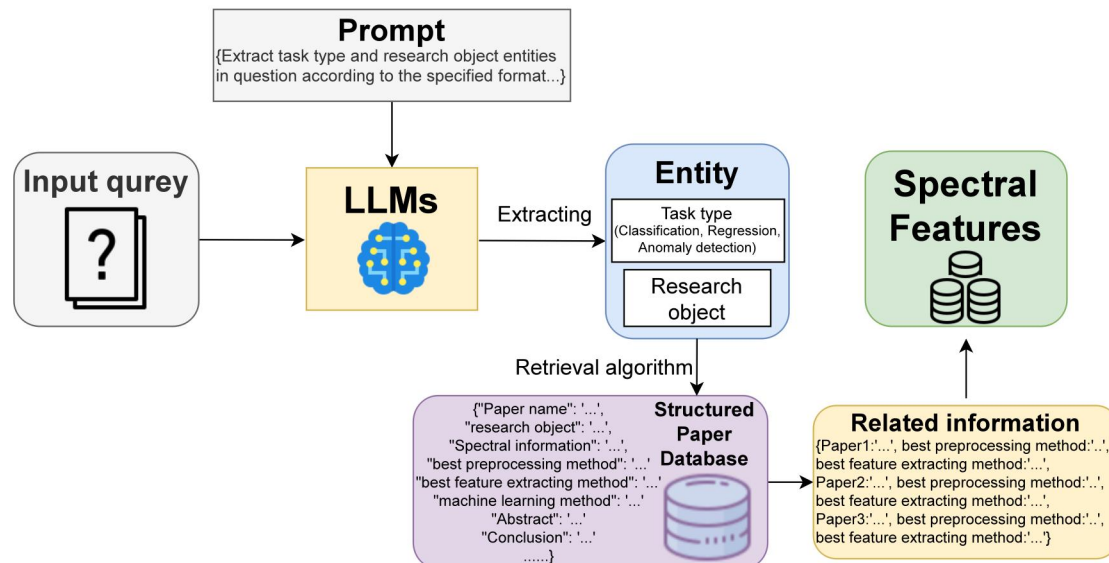


Figure 2. The specific process of entity extraction and knowledge retrieval

2.3 LLM Agent for Spectral Preprocessing and Feature Extraction

The LLM agent drives spectral data conditioning and representation by translating structured metadata from the knowledge base into an interactive methodology selection framework. Upon receipt of a raw absorbance spectrum and the task type entity (classification, anomaly detection, or regression), the agent compiles a comprehensive list of all preprocessing and feature extraction routines reported for analogous materials. In a multi turn dialogue, it presents succinct descriptions of each candidate method including its theoretical rationale, applicable wavelength intervals, and key hyperparameters and solicits the user's preference. Once a method is selected or its parameters refined, the agent invokes the corresponding algorithm from the spectral analysis library, validates the output against predefined quality assurance metrics, and, if necessary, repeats the selection or parameter tuning step until satisfactory spectral quality is achieved.

Baseline correction is offered via the asymmetric least squares (AsLS) algorithm, which estimates the corrected spectrum z by minimizing[12].

$$\sum_{i=1}^n (y_i - z_i)^2 + \lambda \sum_{i=2}^n (z_{i+1} - 2z_i + z_{i-1})^2, \quad (1)$$

where y_i denotes the raw intensity at index i , z_i the baseline subtracted intensity, and λ a smoothing penalty that balances fidelity to the original spectrum against baseline smoothness.

Spectral smoothing is performed with the Savitzky-Golay filter, which fits a polynomial of degree over a moving window of width $2m + 1$ and computes the smoothed value[13].

$$\hat{y}_i = \sum_{j=-m}^m c_j y_{i+j} \quad (2)$$

where the convolution coefficients c_j arise from the least squares fit of the local polynomial.

Normalization options include min-max scaling, which linearly rescales the intensities as

$$y'_i = \frac{y_i - \min_k y_k}{\max_k y_k - \min_k y_k} \quad (3)$$

and the standard normal variate (SNV) transform[14], which centers and scales each spectrum by its own statistics:

$$y''_i = \frac{y_i - \bar{y}}{\sigma_y} \quad (4)$$

with \bar{y} and σ_y representing the mean and standard deviation of the spectrum, respectively.

When derivative spectra are required, the first derivative is approximated by

$$y_i^{(1)} = \frac{y_{i+1} - y_{i-1}}{2\Delta\lambda} \quad (5)$$

and the second derivative by

$$y_i^{(2)} = \frac{y_{i+1} - 2y_i + y_{i-1}}{\Delta\lambda^2} \quad (6)$$

where $\Delta\lambda$ is the uniform wavelength increment.

After preprocessing, the agent offers principal component analysis (PCA), partial least squares (PLS) regression, continuous wavelet transform (CWT), and a Lambert-Beer-Pearson correlation approach as feature extraction strategies[15]. PCA is realized by solving the eigenvalue problem.

$$Cu_k = \lambda_k u_k, \quad C = \frac{1}{n-1} X^T X \quad (7)$$

where X is the preprocessed data matrix, u_k are the principal directions, and λ_k their variances. PLS iteratively derives latent scores by maximizing covariance between the predictor matrix X and response vector y , extracting weight vectors w and loadings p, q through

$$\max_{\|w\|=1} \text{Cov}(Xw, y), \quad X \leftarrow X - tp^T, \quad y \leftarrow y - tc \quad (8)$$

where $t = Xw$, $u = yq$, and c is the loading on y . The CWT is computed as

$$W(a, b) = \frac{1}{\sqrt{a}} \int_{-\infty}^{\infty} y(\lambda) \psi\left(\frac{\lambda - b}{a}\right) d\lambda \quad (9)$$

with scale a , translation b , and mother wavelet ψ .

In scenarios where a small set of reference spectra with known analyte concentrations is available, such as calibration of chemical oxygen demand or quantification of specific compound concentrations, the agent can instead invoke a hybrid Lambert-Beer-Pearson method[16]. Here, the absorbance at each wavelength λ is first computed via the Lambert-Beer law,

$$A(\lambda) = \log \frac{I_0(\lambda)}{I(\lambda)} \quad (10)$$

where I_0 is the incident light intensity and I the transmitted intensity. These absorbance spectra are then compared against each reference curve $R_{ij}(\lambda)$ by computing the Pearson correlation coefficient

$$r_j = \frac{\sum_i (A_i - \bar{A})(R_{ij} - \bar{R}_j)}{\sqrt{\sum_i (A_i - \bar{A})^2} \sqrt{\sum_i (R_{ij} - \bar{R}_j)^2}} \quad (11)$$

The top n coefficients $\{r_j\}$ serve as features that capture both the linear absorbance behavior and the spectral similarity to calibration standards.

By iteratively cycling through user guided method selection, algorithm execution, and quality assurance validation, the LLM agent ensures that each spectrum is processed and represented in accordance with both domain expert practices and the user's experimental objectives, thereby furnishing optimal inputs for the downstream inference tasks. Figure 3 shows the specific process of preprocessing and feature extracting.

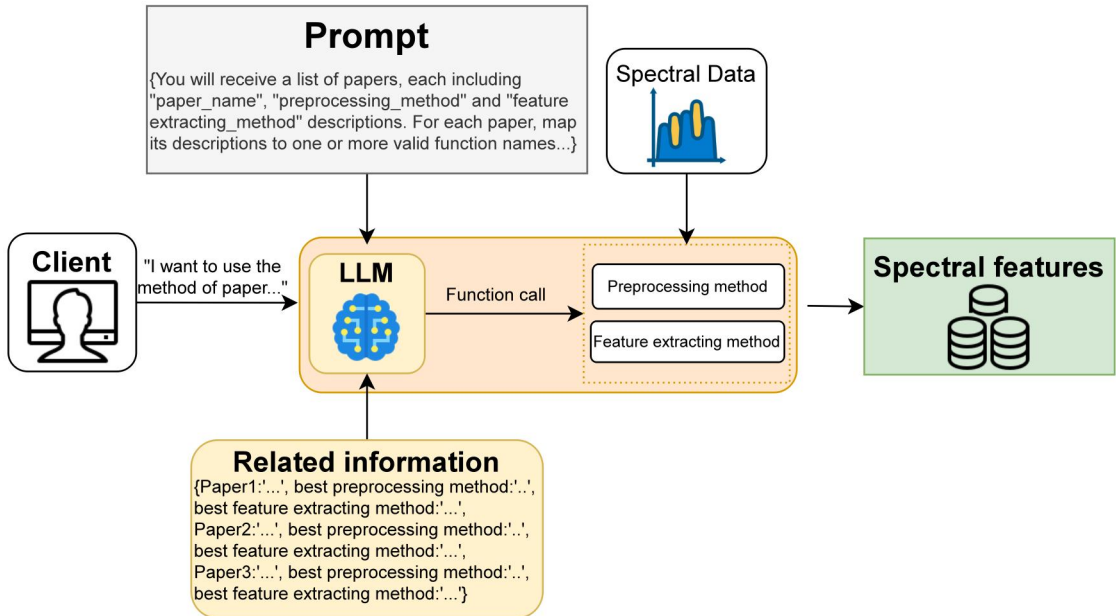


Figure 3. The specific process of preprocessing and feature extracting

2.4 LLM multi Task Reasoning Pipeline

To perform simultaneous classification, anomaly detection, and regression on spectral data, the LLM agent embeds the task type entity obtained during entity retrieval into each prompt, thereby guiding the model's decision strategy. The complete dataset for each material class is first partitioned into training, validation, and test subsets. During the training phase, representative samples and their true labels are supplied directly within the prompt as exemplars, enabling the LLM to ground its reasoning in observed spectra feature and known outcomes. In the subsequent multi turn validation phase, the agent submits the entire validation subset to the LLM in each round, requesting task specific predictions: for classification the predicted subclass label, for anomaly detection a binary flag $\bar{y}_i \in \{0,1\}$, and for regression a continuous concentration or property value $\bar{y}_i \in \mathbb{R}$.

Figure 4 shows the specific process of LLM multi task Reasoning.

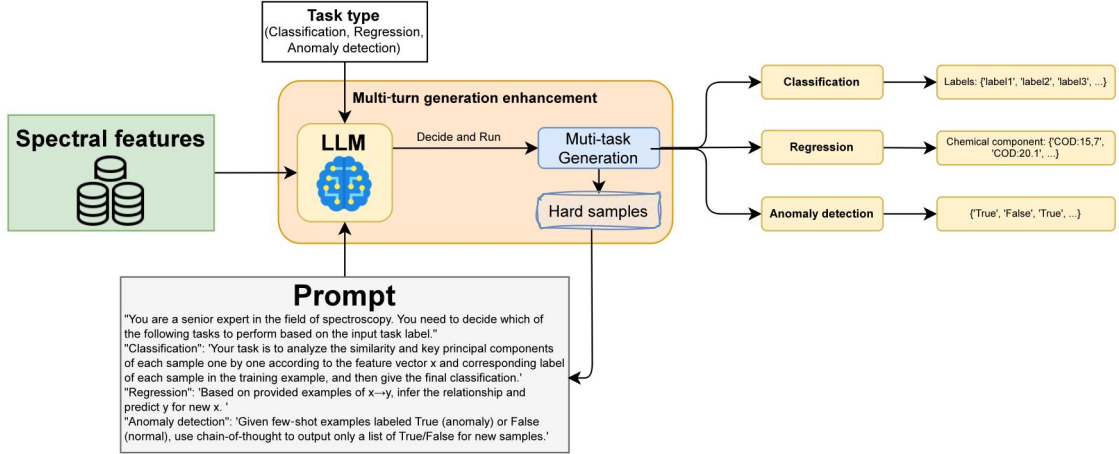


Figure 4. The specific process of LLM multi Task Reasoning

After each reasoning turn t , performance metrics are computed according to standard definitions. For the classification task, accuracy is given by

$$Accuracy^{(t)} = \frac{1}{N_{val}} \sum_{i=1}^{N_{val}} \mathbf{1}(\hat{y}_i^{(t)} = y_i) \quad (12)$$

where N_{val} is the number of validation samples, $\hat{y}_i^{(t)}$ the model's prediction on sample i at turn t and y_i its ground truth label.

For the anomaly detection task, the area under the receiver operating characteristic curve (AUC) is employed, defined as

$$AUC^{(t)} = \frac{1}{N_{pos}N_{neg}} \sum_{i:y_i=1} \sum_{j:y_j=0} \mathbf{1}(s_i^{(t)} > s_j^{(t)}) \quad (13)$$

where N_{pos} and N_{neg} denote the numbers of anomalous and normal samples respectively, and $s_i^{(t)}$ the predicted anomaly score. For the regression task, the coefficient of determination is computed as

$$R^2(t) = 1 - \frac{\sum_{i=1}^{N_{val}} (y_i - \hat{y}_i^{(t)})^2}{\sum_{i=1}^{N_{val}} (y_i - \bar{y})^2} \quad (14)$$

with \bar{y} denoting the mean of the true responses over the validation set.

At the end of each round, the agent identifies "hard samples" as those for which $(\hat{y}_i^{(t)} \neq y_i)$ (classification), those that contribute most to the AUC error (anomaly detection), or those with large residuals $|y_i - \hat{y}_i^{(t)}| > \epsilon$ (regression), where ϵ is a task specific tolerance. These challenging cases, along with their true labels or scores, are appended to the prompt for the next iteration, thereby iteratively enriching the context with the most informative examples. In each successive turn, the LLM refines its reasoning by contrasting prior predictions with actual outcomes. This iterative feedback continues until convergence, defined by

$$Metric^{(t)} - Metric^{(t-1)} < \delta \quad (15)$$

where $Metric$ denotes Accuracy, AUC, or R^2 as appropriate, and δ is a small positive threshold.

This reasoning paradigm diverges fundamentally from conventional machine learning and deep learning training schemes in that the model's internal parameters remain fixed throughout. Instead of weight updates, the entire dataset which is partitioned into training, validation and test subsets is encoded directly into the prompt. During each reasoning turn, the LLM effectively undergoes prompt tuning: exemplars from the training set anchor its task specific inference, validation predictions guide the selection of hard cases, and those challenging examples are appended to the prompt for subsequent turns. In this way, the model acquires tailored reasoning capabilities for the particular spectral task and dataset without gradient based optimization. The

learned behavior resides entirely within the expanded, multi turn prompt context, which serves as a dynamic instruction set enabling the base LLM to perform domain adapted inference while preserving its original weights.

Upon convergence, the final prompt now containing the original training exemplars, selected preprocessing and feature extraction descriptions, and a curated set of hard samples is used to generate predictions for the test set. This multi turn, feedback driven reasoning pipeline ensures that the LLM agent not only learns from representative examples but also adapts dynamically to the most informative error cases, thereby maximizing robustness and generalization across classification, anomaly detection, and regression tasks.

3. Results and discussion

3.1 Experiment settings

All experiments were conducted on a workstation equipped with an NVIDIA GeForce RTX 4070 Ti Super GPU with 16 GB of memory, and all LLM calls were performed via API. For the entity extraction stage, we evaluated both the qwen-turbo (version 2025-02-11) and qwen-plus (version 2025-01-25) models, whereas the multi task reasoning pipeline exclusively employed qwen-plus. During entity extraction, the LLM temperature was set to 0.1 to encourage precise identification of research objects and task types. In the multi task inference phase, a temperature of 0.5 was adopted uniformly to balance creativity and stability across classification, anomaly detection, and regression outputs and the maximum number of rounds of multi turn conversational enhanced reasoning is 5 rounds.

To assess anomaly detection performance, we report both the area under the receiver operating characteristic curve (AUC) and precision, while regression accuracy is quantified by the coefficient of determination R^2 and the root mean square error (RMSE). Each multi turn reasoning experiment was repeated ten times for each material category, and results are presented as the mean \pm standard deviation. In order to remain within the maximum token limits imposed by the LLM API, the total dataset size was restricted to 80 samples per material. Each dataset was partitioned according to a 4:2:2 ratio for training, validation, and testing.

3.2 Experiments of entity extraction and knowledge retrieval

3.2.1 Entity extraction accuracy

The performance of the entity extraction and subsequent knowledge retrieval modules was evaluated in order to assess the system's ability to identify both the research object and the analysis task from queries, and to retrieve the appropriate structured entries from the spectral literature corpus. For the entity extraction evaluation, a set of one hundred questions was manually constructed, covering three task types (classification, anomaly detection, regression) across five material categories. Each question was annotated with the ground truth research object label and task type label prior to testing. The prompts for entity extraction were then submitted to the qwen-turbo and qwen-plus models via API, with the research object entity evaluated using a fuzzy matching criterion (FuzzyWuzzy) and the task type entity assessed by exact match accuracy[17].

Table 2 Evaluation results of entity extraction

Models	Acc(Research object)	Acc(Task type)
qwen-turbo	82	89
qwen-plus	86	100

The results, summarized in Table 2, indicate that qwen-plus outperformed qwen-turbo on both metrics. Specifically, qwen-plus achieved an accuracy of 86% for extracting research object, compared to 82% for qwen-turbo, and correctly identified the task type in all cases (100% accuracy), whereas qwen-turbo attained 89% on this metric. These findings demonstrated that the enhanced language understanding capabilities of qwen-plus yield more precise entity recognition, particularly for distinguishing among closely related spectral materials.

Following successful entity extraction, the identified labels of research objects were used to query the structured knowledge base via retrieval algorithms. Manual inspection of a subset of retrieval outputs confirmed that over 90% of the

top-ranked documents contained metadata entries corresponding to the intended material, thereby validating the robustness of the retrieval pipeline. This end-to-end evaluation of entity extraction and knowledge retrieval establishes a reliable foundation for the downstream multi task reasoning agents.

3.2.2 Retrieval effectiveness

In this study, three established lexical retrieval models were employed to identify relevant publications from the structured corpus: the Bag of Words (BoW) model, BM25, and TF-IDF cosine similarity. The BoW model represents each document as an unordered multiset of word frequencies, disregarding syntactic structure and term dependencies[18]. While straightforward to implement, its inability to capture contextual nuances often yields suboptimal precision in specialized domains. BM25, or Best Matching 25, builds upon the probabilistic retrieval framework by incorporating term frequency saturation, document length normalization, and inverse document frequency weighting; it has become a de facto standard in information retrieval for its balanced treatment of term importance and document verbosity[19]. The TF-IDF cosine similarity approach combines classical term frequency inverse document frequency weighting with a vector space model, measuring the cosine of the angle between query and document vectors to quantify their alignment; this method effectively emphasizes domain specific vocabulary while mitigating the influence of overly common terms.

Retrieval performance was evaluated on a curated test corpus of 200 documents sampled from the full SDAAP repository. This subset comprised ten publications on ink spectroscopy, twenty on water quality spectroscopy, ten on traditional Chinese medicine spectroscopy, ten on Pu'er tea spectroscopy, and 150 papers concerning unrelated substances to serve as noise. One hundred queries were derived from the standardized research object labels produced in Section 3.2.1. For each query, the three highest ranked documents were retrieved by each model and compared against a set of preassigned relevance labels. Retrieval precision was calculated as the fraction of correctly retrieved documents among the top three for each query, and the mean precision across all queries was reported.

Table 3 Evaluation results of knowledge retrieval

Methods	Accuracy(%)
Bag of Words model	56.00
BM25	80.67
TF-IDF cosine similarity retrieval method	81.33

Table 3 summarizes the quantitative outcomes of these retrieval experiments. As shown, the Bag of Words model approach achieved a mean precision of 56.00%, reflecting the limitations of raw term counts in this specialized domain. The TF IDF model produced a substantially higher mean precision of 81.33%, demonstrating the benefit of inverse document frequency weighting in discriminating domain specific terms. BM25 attained a comparable mean precision of 80.67%, indicating that its term frequency saturation and document length normalization confer performance similar to TF IDF under these pilot conditions. Together, these results confirm that weighted retrieval schemes markedly outperform the unweighted Bag of Words approach in identifying relevant spectral analysis literature within a noisy corpus.

3.3 Spectral Preprocessing and Feature Extraction Outcomes

The specific preprocessing and feature extraction routines applied to each material, drawn from the structured literature metadata, are summarized in Table 4. Stamp pad ink spectra were smoothed using a Savitzky Golay filter and then subjected to standard normal variate transformation before extracting principal components. Traditional Chinese medicine samples employed SNV followed by first derivative filtering to enhance resolution of overlapping bands, with subsequent PCA. Citri Reticulatae Pericarpium spectra underwent a combined Savitzky Golay derivative and SNV workflow prior to dimensionality reduction by PCA, while Pu'er tea samples were processed by SNV alone before PCA. Wastewater spectra were baseline corrected and then transformed into Pearson correlation features against reference COD profiles.

Table 4 Retrieval results for experimental material related preprocessing methods and feature extraction methods

Materials	Preprocess method	Feature extract method
Ink	SG+SNV	PCA
Chinese medicine	SNV+FD	PCA
CRP	SGFD+SNV	PCA
Pu'er tea	SNV	PCA
Waste water	BC	Pearson correlation features

Figure 5 illustrates, for each material, the original absorbance profile alongside the processed spectrum after the selected literature guided methods and feature extraction. In stamp pad ink (Figure 5a), the smoothing step clearly attenuates high frequency noise while SNV aligns spectral baselines, yielding a more uniform band shape. For Chinese medicine (Figure 5b), first derivative filtering accentuates subtle inflections corresponding to overlapping chemical constituents. The CRP spectra (Figure 5c) exhibit both noise reduction and peak sharpening from the combined Savitzky Golay derivative and SNV treatment. In Pu'er tea (Figure 5d), SNV alone effectively corrects for path length variations, producing spectra with reduced scatter. Finally, the wastewater absorbance curve (Figure 5e) demonstrates the removal of baseline drift by asymmetric least squares, preparing the profile for subsequent Pearson based feature encoding. Together, these results confirm that the agent's metadata driven selection of preprocessing and extraction protocols yields well conditioned, low dimensional representations optimized for the downstream inference tasks.

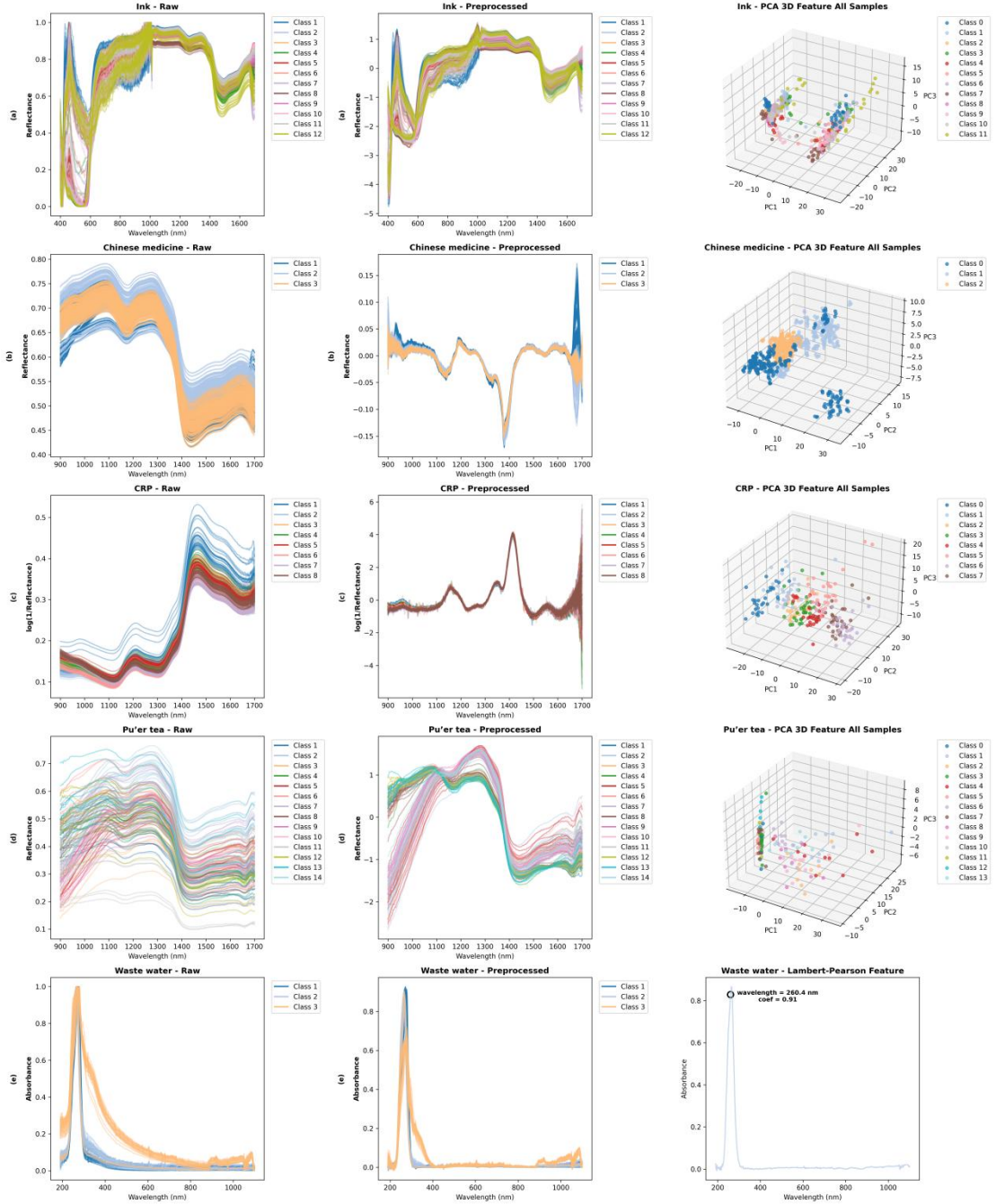


Figure 5. Raw spectra, preprocessed spectra, and resulting feature maps for five material categories: (a) Stamp-pad ink, (b) Chinese medicine, (c) Citri Reticulatae Pericarpium, (d) Pu'er tea, and (e) Wastewater.

3.4 Results of multi task reasoning

3.4.1 Classification

This task aims to evaluate the capability of different models to accurately classify spectroscopic samples from four material categories: stamp pad ink, Chinese medicinal materials, Citri Reticulatae Pericarpium (CRP), and Pu'er tea. Each sample's input comprises raw spectral data subjected to category specific optimal preprocessing techniques, followed by feature extraction using principal component analysis (PCA) with five retained components. These low dimensional spectral features were used as inputs for both LLM based models and classical machine learning classifiers.

We employed two LLM based approaches: a single turn inference model using exemplar augmented prompts and a multi turn variant that integrates iterative feedback from difficult samples to progressively refine classification boundaries. As baselines,

three classical classifiers were tested: support vector machine (SVM)[20], k-nearest neighbors (KNN)[21], and random forest (RF) which are all trained on the same features extracted by PCA[22]. We further evaluated a one dimensional convolutional neural network (CNN)[23] and a simple Transformer encoder[24], both trained on the raw, preprocessed spectral vectors.

Table 5 Experiment results of classification task

Methods	Ink Acc. (%)	Chinese medicine Acc. (%)	CRP Acc. (%)	Pu'er tea Acc. (%)
LLM(single)	64.4 \pm 6.3	86.668 \pm 16.328	100 \pm 0	38 \pm 4
LLM(multi)	72.2 \pm 3.9	93.334\pm13.332	100\pm0	49\pm3.741
SVM	76.666 \pm 4.158	66.67 \pm 0	100 \pm 0	41 \pm 7.348
KNN	62.222 \pm 5.442	66.67 \pm 0	100 \pm 0	26 \pm 3.742
RF	82.222\pm4.156	39.998 \pm 13.336	87.5 \pm 0	40 \pm 4.472
CNN	35.6 \pm 5	33.3 \pm 0	28.8 \pm 5.6	23 \pm 7.6
Transformer	74.4 \pm 8.4	37.8 \pm 9.9	91.3 \pm 3.4	21 \pm 6.5

Table 5 summarizes the classification results. The multi turn LLM achieved a notable improvement over its single turn counterpart across all materials. For Chinese medicine, accuracy rose from 86.7 \pm 16.3 % in the single turn setup to 93.3 \pm 13.3 % with multi turn prompting, surpassing all classical and deep learning models: SVM and KNN both plateaued at 66.7 %, RF lagged at 40.0 \pm 13.3 %, CNN reached only 33.3 \pm 0 %, and the Transformer encoder 37.8 \pm 9.9 %. This underscores the LLM's ability to leverage exemplar guidance in distinguishing spectrally similar subclasses where both shallow networks and classical methods struggle.

Similarly, for Pu'er tea, multi turn prompting improved accuracy to 49.0 \pm 3.7 %, exceeding the single turn LLM and other models. In contrast, CRP classification proved trivial for all approaches, each achieving perfect accuracy (100.0 \pm 0 %), reflecting the highly distinctive nature of its spectral signatures.

For stamp pad ink, the LLM multi turn model reached 72.2 \pm 3.9 %, outperforming the single turn LLM (64.4 \pm 6.3 %), KNN (62.2 \pm 5.4 %), and CNN (35.6 \pm 5.0 %), but still fell short of RF (82.2 \pm 4.2 %) and SVM (76.7 \pm 4.2 %). The Transformer encoder delivered 74.4 \pm 8.4 %, indicating that, for certain materials with pronounced features, even lightweight deep learning models can match or exceed LLM performance.

Overall, these results demonstrate that LLM based classification benefits significantly from multi turn interaction, particularly in spectrally ambiguous or heterogeneous datasets where direct prompt based classification and shallow networks are insufficient. However, in cases of clear spectral separability or when sample size permits, traditional ensemble methods and simple deep learning architectures can still deliver superior or comparable performance. The reduced standard deviation observed in multi turn LLM predictions further highlights its robustness and consistency, emphasizing the advantage of iterative reasoning for reliable spectral classification.

3.4.2 Regression

This study evaluates the prediction of chemical oxygen demand (COD) for three separate wastewater matrices effluent water, river water, and influent water using spectroscopic inputs that have been preprocessed and reduced to three features via a Lambert-Beer absorbance and Pearson correlation procedure. Each sample is thus represented by a concise three dimensional feature vector reflecting its linear absorbance behavior and similarity to calibration standards.

To benchmark reasoning based inference, two LLM pipelines were compared alongside three classical regressors. The single turn LLM generates COD estimates directly from exemplar augmented prompts, whereas the multi turn LLM iteratively incorporates validation samples with large errors into its prompt context to refine predictions. As parametric baselines, linear regression (LR) assumes a direct linear mapping between the three features and COD, support vector regression (SVR) employs kernel functions to capture nonlinear relationships[25], and partial least squares regression (PLSR) projects features and response into a shared latent space to exploit covariance structure[26]. We further evaluated a one dimensional convolutional neural

network (CNN) and a compact Transformer encoder, both trained directly on the raw, preprocessed spectra without manual feature reduction.

Table 6 Experiment results of regression task

Type	Methods	R2	RMSE
Effluent water	LLM(single)	0.499 \pm 0.114	7.42 \pm 1.904
	LLM(multi)	0.737\pm0.056	5.769\pm1.114
	LR	0.457 \pm 0.159	7.771 \pm 2.552
	SVR	0.031 \pm 0.059	10.484 \pm 3.09
	PLSR	0.463 \pm 0.169	7.729 \pm 2.65
	CNN	-3.426 \pm 0.181	20.129 \pm 0.415
	Transformer	-1.193 \pm 0.068	14.171 \pm 0.217
River water	LLM(single)	0.783 \pm 0.068	2.336 \pm 0.288
	LLM(multi)	0.816\pm0.063	2.121\pm0.306
	LR	0.813 \pm 0.13	2.179 \pm 0.87
	SVR	0.74 \pm 0.063	2.629 \pm 0.34
	PLSR	0.85\pm0.07	1.975\pm0.556
	CNN	-10.475 \pm 2.196	17.042 \pm 1.514
	Transformer	-3.318 \pm 0.504	10.547 \pm 1.426
Influent water	LLM(single)	0.878 \pm 0.014	13.926 \pm 0.783
	LLM(multi)	0.918\pm0.005	11.551\pm1.124
	LR	0.741 \pm 0.025	20.281 \pm 0.976
	SVR	0.239 \pm 0.047	34.746 \pm 1.062
	PLSR	0.737 \pm 0.027	20.424 \pm 1.025
	CNN	-1.198 \pm 0.005	101.62 \pm 0.124
	Transformer	-0.928 \pm 0.055	95.159 \pm 1.366

Table 6 reports the mean \pm standard deviation of the coefficient of determination (R^2) and root mean square error (RMSE) over ten repeated trials for each water type. For effluent samples, single turn LLM achieved $R^2=0.499 \pm 0.114$ with RMSE = 7.42 \pm 1.90, while the multi turn strategy improved to $R^2=0.737 \pm 0.056$ and RMSE = 5.77 \pm 1.11. Linear regression and PLSR yielded similar but lower performance on this heterogeneous dataset ($R^2 \approx 0.46$, RMSE \approx 7.75), and SVR failed to generalize ($R^2=0.031 \pm 0.059$, RMSE = 10.48 \pm 3.09). In river water, all methods performed strongly; multi turn LLM ($R^2=0.816 \pm 0.063$, RMSE = 2.12 \pm 0.31) closely matched PLSR ($R^2=0.850 \pm 0.070$, RMSE = 1.98 \pm 0.56) and LR ($R^2=0.813 \pm 0.130$, RMSE = 2.18 \pm 0.87), with SVR remaining competitive ($R^2=0.740 \pm 0.063$, RMSE = 2.63 \pm 0.34). For influent spectra, multi turn LLM led with $R^2=0.918 \pm 0.005$ and RMSE = 11.551 \pm 1.124, outperforming LR and PLSR ($R^2 \approx 0.74$, RMSE \approx 20.5) and markedly surpassing SVR ($R^2=0.239 \pm 0.047$, RMSE = 34.746 \pm 1.062). In contrast, the CNN and Transformer both produced negative R^2 values and high RMSE, indicating that shallow deep learning architectures struggle to generalize from a small input space without extensive parameter tuning.

The results indicate that the multi turn LLM's iterative integration of difficult samples substantially improves COD estimation in complex effluent and influent matrices, reducing prediction error by more than 20%. In river water, where the spectral concentration relationship is inherently more linear and less noisy, classical LR and PLSR remain highly competitive. SVR's inconsistent performance across all water types underscores the challenge of kernel based regression under small sample conditions. Overall, coupling Lambert-Beer-Pearson feature extraction with knowledge guided LLM reasoning delivers a flexible and effective framework for spectroscopic COD prediction across diverse water matrices.

3.4.3 Anomaly Detection

This task investigates anomaly detection across four spectroscopic material categories: ink, Chinese medicine, Citri Reticulatae Pericarpium (CRP), and Pu'er tea. The input for each sample comprises spectroscopic data that has been preprocessed using the optimal spectral transformation for its material class, followed by dimensionality reduction via principal component analysis (PCA) with five components. This results in a five dimensional spectral feature vector per sample, which serves as the input to all models under evaluation.

For each material, a subclass was designated as the reference class and considered "normal," comprising 60% of the data. The remaining 40% was divided into two types of anomalies: 20% were taken from different subclasses (inter class anomalies), and 20% were generated by applying small perturbations to the reference data (intra class anomalies). All normal samples were labeled as True, while both anomaly types were labeled False. The model's task is to perform binary classification for each spectrum, indicating whether it conforms to the learned "normal" distribution. Evaluation metrics included precision and the area under the receiver operating characteristic curve (AUC), which together reflect detection accuracy and robustness under class imbalance.

We compared two variants of a LLM based approach: a single turn model that makes direct predictions from exemplar prompts, and a multi turn agent that iteratively incorporates hard cases samples for which the model's confidence is low into the prompt for refinement. Three classical one class anomaly detection models were also considered: Isolation Forest (IF), which uses random partitioning to isolate anomalies[27]; one class support vector machine (OC-SVM), which attempts to separate the origin from the data in feature space using a hyperplane[28]; and one class random forest (OC-RF), an ensemble method trained only on normal data[29]. To evaluate lightweight deep learning alternatives, we also tested an autoencoder trained on the normal class and an LSTM autoencoder cascade[30][31], both using the same spectral features.

Table 7 Experiment results of anomaly detection task

Methods	Ink		Chinese medicine		CRP		Pu'er tea	
	Precision	AUC	Precision	AUC	Precision	AUC	Precision	AUC
LLM(single)	0.613 \pm 0.211	0.599 \pm 0.052	0.24 \pm 0.219	0.49 \pm 0.037	0.780 \pm 0.16	0.736 \pm 0.139	0.833 \pm 0.139	0.699 \pm 0.131
LLM(multi)	0.768 \pm 0.192	0.706 \pm 0.051	0.83 \pm 0.264	0.743 \pm 0.151	0.933 \pm 0.082	0.843 \pm 0.037	0.9 \pm 0.122	0.733 \pm 0.103
IF	0.534 \pm 0.085	0.656 \pm 0.047	0.43554 \pm 0.109	0.547 \pm 0.097	0.810 \pm 0.097	0.793 \pm 0.033	0.796 \pm 0.170	0.600 \pm 0.081
OC-SVM	0.686 \pm 0.196	0.643 \pm 0.079	0.52 \pm 0.04	0.617 \pm 0.021	0.720 \pm 0.051	0.687 \pm 0.038	0.775 \pm 0.133	0.686 \pm 0.154
OC-RF	0.433 \pm 0.388	0.513 \pm 0.093	0.61906 \pm 0.131	0.65 \pm 0.075	0.655 \pm 0.194	0.53 \pm 0.123	0.45 \pm 0.266	0.473 \pm 0.121
Autoencoder	0.4 \pm 0.548	0.503 \pm 0.073	0.8 \pm 0.447	0.557 \pm 0.06	0.8 \pm 0.447	0.547 \pm 0.082	0.8 \pm 0.447	0.592 \pm 0.154
LSTM+Autoencoder	0.4 \pm 0.548	0.503 \pm 0.073	0.6 \pm 0.548	0.53 \pm 0.073	0.6 \pm 0.548	0.51 \pm 0.1	0.6 \pm 0.548	0.508 \pm 0.16

As summarized in Table 7, the multi turn LLM consistently outperformed its single turn counterpart across all material categories. For CRP, multi turn prompting led to a significant improvement in both precision (0.933 \pm 0.082) and AUC (0.843 \pm 0.037), highlighting the model's ability to refine its anomaly boundary through iterative contextualization when the spectral differences are subtle. Similarly, for Chinese medicine, multi turn prompting boosted precision from 0.24 \pm 0.219 to 0.83 \pm 0.264, suggesting that LLM based reasoning is particularly effective in domains with fine grained spectral variability.

Classical detectors such as Isolation Forest and OC-SVM achieved moderate performance but lacked the adaptability to nuanced outliers. OC-RF exhibited high variance and underwhelming AUC, indicating instability under limited anomaly examples. The autoencoder and LSTM autoencoder, despite their representational flexibility, failed to surpass random forest baselines; their high standard deviations and modest AUC scores suggested that neural reconstructions of normal patterns alone are insufficient for robust anomaly discrimination without extensive training data.

3.5 Ablation study

3.5.1 Temperature

The temperature parameter in large language models controls the randomness of token sampling: lower values bias generation toward the most probable continuations, yielding more deterministic outputs, while higher values promote exploration of less likely tokens, increasing variation at the expense of consistency. All experiments in this ablation study employed the qwen-plus model, with dataset splits and model architecture held constant; only the temperature was varied among 0.3, 0.5, and 0.7. Both single turn inference and the multi turn feedback pipeline were evaluated on ink classification, influent water regression, and anomaly detection for Chinese medicine.

Table 8 Experiments results of different temperature

Temperature	Classification (Ink)		Regression (Influent water)		Anomaly detection (Chinese medicine)	
	Acc (%)	R2	RMSE	Precision	AUC	
0.3 (single)	61.1 \pm 13.6	0.9 \pm 0.011	16.805 \pm 0.907	0.28 \pm 0.259	0.503 \pm 0.106	
0.3 (multi)	77.8\pm6.8	0.918 \pm 0.004	15.138 \pm 0.456	0.85 \pm 0.224	0.753 \pm 0.095	
0.5 (single)	64.4 \pm 6.3	0.878 \pm 0.014	13.926 \pm 0.783	0.24 \pm 0.219	0.49 \pm 0.037	
0.5 (multi)	72.2 \pm 3.9	0.918\pm0.005	11.551\pm1.124	0.83 \pm 0.264	0.743 \pm 0.151	
0.7 (single)	63.3 \pm 9.3	0.866 \pm 0.029	19.327 \pm 2.139	0.32 \pm 0.179	0.483 \pm 0.075	
0.7 (multi)	67.8 \pm 6.1	0.92 \pm 0.007	14.863 \pm 0.854	0.86\pm0.129	0.807\pm0.07	

The results in Table 8 summarize mean performance and standard deviations over ten trials. For ink classification, the highest accuracy ($77.8 \pm 6.8\%$) occurred at temperature = 0.3 in the multi turn setting; increasing temperature systematically degraded classification consistency. In influent regression, the multi turn pipeline achieved its lowest RMSE (11.55 ± 1.12) and strong R^2 (0.918 ± 0.005) at temperature = 0.5, whereas temperature = 0.7 increased error despite marginal gains in R^2 . For anomaly detection on Chinese medicine, the AUC peaked at temperature = 0.7 in the multi turn mode (0.807 ± 0.070), suggesting that a greater sampling diversity can help uncover subtle outliers when guided by iterative feedback.

The observed trends reflect the trade off between determinism and diversity. For classification, lower temperature enhances output stability, allowing the LLM to consistently apply learned spectral distinctions. In regression, a moderate temperature (0.5) balances the need for varied hypothesis exploration with reliable quantitative mapping, yielding the best error reduction. Conversely, detecting anomalies in complex Chinese medicine spectra benefits from higher temperature, where a broader sampling distribution uncovers atypical spectral patterns that deterministic sampling might overlook. Across all tasks, multi turn interaction amplifies these effects by systematically reinforcing correct predictions and guiding the model to refine its reasoning under each temperature regime.

3.5.2 Size of dataset

To investigate how the quantity of training examples influences the LLM reasoning capability, we held the validation and test sets constant while varying only the number of training samples. Originally, ink classification used 40 training spectra, influent regression 20, and Chinese medicine anomaly detection 20. We reran the multi turn reasoning pipeline with training set sizes of 20, 40, and 60 for classification; 10, 20, and 30 for regression; and 10, 20, and 30 for anomaly detection. Table 8 summarizes the resulting performance.

Table 9 Experiment results of different size of dataset

Task	Size of Training set	Metrics
Classification (Ink)		Acc (%)
	20	53.3 \pm 3
	40	72.2 \pm 3.9
	60	81.1\pm5

Regression (Influent water)		R2	RMSE
	10	0.806 ± 0.024	20.959 ± 1.601
	20	0.918 ± 0.005	11.551 ± 1.124
	30	0.903 ± 0.007	17.648 ± 0.639
Anomaly detection (Chinese medicine)		Precision	AUC
	10	0.72 ± 0.067	0.71 ± 0.022
	20	0.83 ± 0.264	0.743 ± 0.151
	30	0.567 ± 0.091	0.567 ± 0.046

The results in Table 9 reveal that classification accuracy steadily improves as more annotated ink spectra are provided, rising from $53.3 \pm 3.0\%$ at 20 samples to $81.1 \pm 5.0\%$ at 60 samples. This trend underscores the model's reliance on exemplar diversity to sharpen decision boundaries: with additional class instances, the agent gains broader exposure to spectral variability and thus refines its subclass discrimination.

In the influent regression task, performance peaks at 20 training samples ($R^2 = 0.918 \pm 0.005$, RMSE = 11.55 ± 1.12). Fewer examples (10) yield insufficient context, resulting in underfit predictions, while an increase to 30 degrades both R^2 and RMSE likely reflecting overfitting to idiosyncratic spectra or exceeding token length constraints that dilute prompt clarity. Thus, a moderate training set affords the ideal balance between exemplars for pattern learning and prompt coherence for the LLM.

For anomaly detection in Chinese medicinal materials, the optimal performance likewise occurs at 20 samples (precision = 0.83 ± 0.26 , AUC = 0.743 ± 0.15). A smaller set (10) limits the agent's ability to characterize normal spectral patterns comprehensively, reducing outlier discrimination. Conversely, expanding to 30 examples introduces redundant or noisy reference cases that appear to confuse the iterative reasoning process, causing a marked drop in both precision and AUC.

Collectively, these findings indicate that while more training data generally enhances model reasoning by broadening the exemplar base, there exists a task specific threshold beyond which additional samples can conflict with prompt length limits or introduce spectral noise. Careful calibration of training set size is therefore essential to maximize the effectiveness of multi turn LLM inference in spectroscopic applications.

3.5.3 Different LLMs

To evaluate how model architecture and pretraining influence multi task spectral reasoning, we compared four large language models under identical temperature, prompt design, and dataset conditions: The Qwen series developed by Alibaba and accessed via the Alibaba Cloud API includes qwen-plus and qwen-turbo. Both are based on the Transformer architecture and pretrained on massive text and multimodal corpora to generate coherent, semantically rich outputs across domains. Qwen-plus (version 2025-01-25) offers balanced reasoning performance, cost, and latency, making it well suited for moderately complex tasks. Qwen-turbo (version 2025-02-11) prioritizes inference speed and minimal cost at the expense of reasoning depth, targeting simpler tasks[32]. DeepSeek-v3, released on December 26, 2024 by the Chinese AI startup DeepSeek, is a 671 billion parameter mixture of experts model pretrained on 14.8 trillion tokens[33]. Finally, chatgpt-4-turbo, provided by OpenAI, is a high capacity conversational model finetuned for chat applications[34]. What is worth mentioning is that we disabled the thinking function for all models to avoid excessive latency and redundant output during iterative multi turn reasoning. Each model was assessed in both single turn and multi turn configurations on ink classification, influent water regression, and Chinese medicine anomaly detection. The experiment results is shown in Table 10.

Table 10 Experiment results of different LLMs

LLMs	Classification (Ink)		Regression (Influent water)		Anomaly detection (Chinese medicine)	
	Acc (%)	R2	RMSE	Precision	AUC	
qwen-plus(single)	64.4 ± 6.3	0.878 ± 0.014	13.926 ± 0.783	0.24 ± 0.219	0.49 ± 0.037	
qwen-plus(multi)	72.2 ± 3.9	0.918 ± 0.005	11.551 ± 1.124	0.83 ± 0.264	0.743 ± 0.151	

qwen-turbo(single)	28.9 ± 16.4	0.589 ± 0.032	34.027 ± 1.354	0.247 ± 0.152	0.477 ± 0.038
qwen-turbo(multi)	47.8 ± 5	0.797 ± 0.053	25.824 ± 2.505	0.327 ± 0.075	0.5 ± 0.037
deepseek-v3(single)	53.3 ± 29.8	0.867 ± 0.028	19.315 ± 1.959	0.4 ± 0.137	0.507 ± 0.072
deepseek-v3(multi)	76.7 ± 2.5	0.886 ± 0.014	18.79 ± 2.677	0.967 ± 0.075	0.807 ± 0.099
chatgpt-4-turbo(single)	70 ± 5	0.842 ± 0.031	21.037 ± 2.123	0.1 ± 0.137	0.383 ± 0.046
chatgpt-4-turbo(multi)	87.8 ± 4.6	0.884 ± 0.018	21.042 ± 2.257	0.31 ± 0.082	0.48 ± 0.043

The comparative analysis indicates that qwen-plus provides robust, balanced performance across tasks. Its instruction tuned design enables effective refinement in multi turn reasoning, achieving strong gains in classification and regression. Qwen-turbo's lightweight architecture delivers rapid responses but lacks the representational capacity to model complex spectral patterns, resulting in lower accuracy and higher regression error.

DeepSeek-v3's domain adapted mixture of experts structure excels in anomaly detection, achieving the highest precision (0.967 ± 0.075) and AUC (0.807 ± 0.099) by leveraging specialized expert subnetworks to capture subtle outlier signals, though its regression improvements are more modest.

ChatGPT-4-turbo attains the best classification accuracy ($87.8 \pm 4.6\%$), likely due to its extensive pretraining and large context window that facilitate nuanced decision boundaries. Nevertheless, its regression and anomaly detection metrics lag behind qwen-plus and DeepSeek-v3, suggesting that conversational optimization does not directly translate into quantitative estimation or outlier sensitivity without domain specific adaptation.

These findings underscore the importance of model selection aligned with task demands: balanced instruction tuned models excel at multi task reasoning, domain specialized architectures offer superior anomaly detection, and high capacity conversational models can provide cutting edge classification performance at the cost of regression precision.

4. Conclusion

We have presented a unified, LLM driven agent framework for end-to-end IR spectroscopy that seamlessly combines literature guided preprocessing, feature extraction, and multi task reasoning. By harnessing few shot prompting and iterative feedback, the system attains robust performance on classification, regression, and anomaly detection across heterogeneous spectral datasets, outperforming or matching traditional machine learning and simple deep learning baselines with minimal training data. Ablation studies underscore the roles of LLM sampling temperature, exemplar diversity, dataset size, and model selection in optimizing inference quality.

Future work will extend this agent architecture to accommodate image based spectral modalities, incorporating modules for multispectral and hyperspectral imaging. By integrating spatial-spectral feature extraction and domain specific LLM prompting, the enhanced framework will address complex analytical scenarios, such as material mapping and remote sensing, further broadening the applicability of intelligent, automated spectral analysis.

CRediT authorship contribution statement

Zujie Xie: Methodology, Data curation, Validation, Formal analysis, Visualization, Software, Writing. **Zixuan Chen:** Data curation, Validation, Formal analysis, Visualization, Writing. **Jiheng Liang:** Conceptualization, Methodology. **Xiangyang Yu:** Conceptualization, Supervision, Writing. **Ziru Yu:** Conceptualization, Methodology, Supervision, Writing.

Funding Sources

This research did not receive any specific grant from funding agencies in the public, commercial, or not-for-profit sectors.

Reference

[1] Pan, S., Zhang, X., Xu, W., Yin, J., Gu, H., & Yu, X., "Rapid on-site identification of geographical origin and storage age of tangerine peel by near-infrared spectroscopy," *Spectrochimica Acta Part A: Molecular and Biomolecular Spectroscopy* 271 (2022): 120936. <https://doi.org/10.1016/j.saa.2022.120936>.

[2] Yu, Z., & Cui, W., "LSCA-net: A lightweight spectral convolution attention network for hyperspectral image processing," *Computers and Electronics in Agriculture* 215 (2023): 108382. <https://doi.org/10.1016/j.compag.2023.108382>

[3] Zhang, Y.; Vlachos, D. G.; Liu, D.; Fang, H. Rapid Adaptation of Chemical Named Entity Recognition Using Few-Shot Learning and LLM Distillation. *J. Chem. Inf. Model.* 2025, 65 (9), 4334 – 4345. <https://doi.org/10.1021/acs.jcim.5c00248>.

[4] Xing, B., Ying, X., Wang, R. et al. Multi-modal Prompt Alignment with Fine-grained LLM Knowledge for Unsupervised Domain Adaptation. *Int J Comput Vis* (2025). <https://doi.org/10.1007/s11263-025-02497-1>

[5] Jablonka, K. M., Schwaller, P., Ortega-Guerrero, A., & Smit, B., "Leveraging large language models for predictive chemistry," *Nature Machine Intelligence* 6 (2024): 161-169. <https://doi.org/10.1038/s42256-024-00789-z>

[6] Zimmermann, Y., Bazgir, A., Al-Feghali, A., et al., 34 examples of LLM applications in materials science and chemistry: Towards automation, assistants, agents, and accelerated scientific discovery (2025). arXiv. <https://arxiv.org/abs/2505.03049>

[7] Xu, W., Huang, C., Gao, S. et al. LLM-Based Agents for Tool Learning: A Survey. *Data Sci. Eng.* (2025). <https://doi.org/10.1007/s41019-025-00296-9>

[8] Zhu, H., Zhao, Y., Zhao, L., Yang, R., & Han, Z., "Pixel-level spectral aflatoxin B1 content intelligent prediction via fine-tuning large language model (LLM)," *Food Control* 171 (2025): 111071. <https://doi.org/10.1016/j.foodcont.2024.111071>

[9] Liang, J., Yu, X., Hong, W., & Cai, Y. (2024). Information extraction of UV-NIR spectral data in waste water based on large language model. *Spectrochimica Acta Part A: Molecular and Biomolecular Spectroscopy*, 318, 124475. <https://doi.org/10.1016/j.saa.2024.124475>

[10] Liang, J., Yu, Z., Xie, Z., & Yu, X. (2024). A quick, trustworthy spectral knowledge Q&A system leveraging retrieval-augmented generation on LLM. arXiv. <https://arxiv.org/abs/2408.11557>

[11] Wang, B., Xu, C., Zhao, X., et al., MinerU: An open-source solution for precise document content extraction (2024). arXiv. <https://arxiv.org/abs/2409.18839>

[12] Peng, J., Peng, S., Jiang, A., et al., "Asymmetric least squares for multiple spectra baseline correction," *Analytica Chimica Acta* 683, no. 1 (2010): 63-68. <https://doi.org/10.1016/j.aca.2010.08.033>

[13] Zhang, G., Hao, H., Wang, Y., et al., "Optimized adaptive Savitzky-Golay filtering algorithm based on deep learning network for absorption spectroscopy," *Spectrochimica Acta Part A: Molecular and Biomolecular Spectroscopy* 263 (2021): 120187. <https://doi.org/10.1016/j.saa.2021.120187>

[14] Peng, X., Yu, X., Lu, L., et al., "Application of handheld near infrared spectrometer in quality control of traditional Chinese medicine: Rapid screening and quantitative analysis of Lonicerae Japonicae Flos adulteration," *Spectrochimica Acta Part A: Molecular and Biomolecular Spectroscopy* 326 (2025): 125215. <https://doi.org/10.1016/j.saa.2024.125215>

[15] Zhang, X., Gao, Z., Yang, Y., et al., "Rapid identification of the storage age of dried tangerine peel using a hand-held near infrared spectrometer and machine learning," *Journal of Near Infrared Spectroscopy* 30, no. 1 (2022): 31-39. <https://doi.org/10.1177/09670335211072740>

[16] Mäntele, W., & Deniz, E., "UV-VIS absorption spectroscopy: Lambert-Beer reloaded," *Spectrochimica Acta Part A: Molecular and Biomolecular Spectroscopy* 173 (2017): 965-968. <https://doi.org/10.1016/j.saa.2016.09.037>

[17] Wu, W.-Y., "A method for fuzzy string matching," in 2016 International Computer Symposium (ICS) (2016): 380-383. <https://doi.org/10.1109/ICS.2016.0083>

[18] Zhang, Y., Jin, R. & Zhou, ZH. Understanding bag-of-words model: a statistical framework. *Int. J. Mach. Learn. & Cyber.* 1, 43-52 (2010). <https://doi.org/10.1007/s13042-010-0001-0>

[19] Kim, J., Kim, H.-U., Adamowski, J., Hatami, S., & Jeong, H. (2022). Comparative study of term-weighting schemes for environmental big data using machine learning. *Environmental Modelling & Software*, 157, 105536. <https://doi.org/10.1016/j.envsoft.2022.105536>

[20] Sugumar, R., & Suganya, D., "A multi-spectral image-based high-level classification based on a modified SVM with enhanced PCA and hybrid metaheuristic algorithm," *Remote Sensing Applications: Society and Environment* 31 (2023): 100984. <https://doi.org/10.1016/j.rsase.2023.100984>

[21] Mancini, M., Taavitsainen, V.-M., & Rinnan, Å., "Comparison of classification methods performance for defining the best reuse of waste wood material using NIR spectroscopy," *Waste Management* 178 (2024): 321-330. <https://doi.org/10.1016/j.wasman.2024.02.033>

[22] Zhang, X.-W., Chen, Z.-G., & Jiao, F., "Application of the combination method based on RF and LE in near infrared spectral modeling," *Spectrochimica Acta Part A: Molecular and Biomolecular Spectroscopy* 289 (2023): 122247. <https://doi.org/10.1016/j.saa.2022.122247>

[23] Huang, J., He, H., Lv, R., Zhang, G., Zhou, Z., & Wang, X. (2022). Non-destructive detection and classification of textile fibres based on hyperspectral imaging and 1D-CNN. *Analytica Chimica Acta*, 1224, 340238. <https://doi.org/10.1016/j.aca.2022.340238>

[24] He, X., Chen, Y., & Lin, Z. (2021). Spatial-Spectral Transformer for Hyperspectral Image Classification. *Remote Sensing*, 13(3), 498. <https://doi.org/10.3390/rs13030498>

[25] Belousov, A. I., Verzakov, S. A., & Von Frese, J., "Applicational aspects of support vector machines," *Journal of Chemometrics* 16 (2002): 482-489. <https://doi.org/10.1002/cem.744>

[26] Igne, B., Reeves, J. B., McCarty, G., Hively, W. D., Lund, E., & Hurlburgh, C. R., "Evaluation of spectral pretreatments, partial least squares, least squares support vector machines and locally weighted regression for quantitative spectroscopic analysis of soils," *Journal of Near Infrared Spectroscopy* 18, no. 3 (2010): 167-176. <https://doi.org/10.1255/jnirs.883>

[27] Cheng, X., Zhang, M., Lin, S., Zhou, K., Zhao, S., & Wang, H., "Two-stream isolation forest based on deep features for hyperspectral anomaly detection," *IEEE Geoscience and Remote Sensing Letters* 20 (2023): Article 5504205, 1-5. <https://doi.org/10.1109/LGRS.2023.3271899>

[28] Muñoz-Marí, J., Bovolo, F., Gómez-Chova, L., Bruzzone, L., & Camps-Valls, G., "Semisupervised one-class support vector machines for classification of remote sensing data," *IEEE Transactions on Geoscience and Remote Sensing* 48, no. 8 (2010): 3188-3197. <https://doi.org/10.1109/TGRS.2010.2045764>

[29] de Santana, F. B., Borges Neto, W., & Poppi, R. J., "Random forest as one-class classifier and infrared spectroscopy for food adulteration detection," *Food Chemistry* 293 (2019): 323-332. <https://doi.org/10.1016/j.foodchem.2019.04.073>

[30] Li, Y., Huang, X., Li, J., Du, M., & Zou, N., "SpecAE: Spectral autoencoder for anomaly detection in attributed networks,"

in Proceedings of the 28th ACM International Conference on Information and Knowledge Management (CIKM '19) (2019): 2233-2336. ACM. <https://doi.org/10.1145/3357384.3358074>

[31] Provotor, O. I., Linder, Y. M., & Veres, M. M., "Unsupervised anomaly detection in time series using LSTM-based autoencoders," in 2019 IEEE International Conference on Advanced Trends in Information Theory (ATIT) (2019): 513-517. IEEE. <https://doi.org/10.1109/ATIT49449.2019.9030505>

[32] Alibaba Cloud . Qwen 2.5-Max: A large language model for advanced reasoning and domain-specific applications. Available from: <https://chat.qwenlm.ai/>. Accessed: 15 June 2025.

[33] DeepSeek . DeepSeek. Available from: <https://www.deepseek.com/>. Accessed: 15 June 2025.

[34] OpenAI. GPT-4. Available from: <https://chatgpt.com/>. Accessed: 15 June 2025.